Surface & Coatings Technology 205 (2011) 4329–4334

Contents lists available at ScienceDirect

Surface & Coatings Technology

journal homepage: www.elsevier.com/locate/surfcoat

Deposition and characterization of Si_xC_{1-x}/Al_2O_3 coatings by magnetron sputtering for nuclear fusion applications

Binbin Song, Ping Wu *, Sen Chen, Murad Ali Khaskheli, Liang Liang

Department of Physics, School of Applied Science, University of Science and Technology Beijing, 30 Xueyuan Road, Haidian District, Beijing 100083, China

ARTICLE INFO

Article history:
Received 1 November 2010
Accepted in revised form 22 March 2011
Available onlline 9 April 2011

Keywords:
Si_xC_{1-x}/Al_2O_3 coating
Growth mode
Structure
Hardness
Adhesion

ABSTRACT

Al_2O_3 coatings were fabricated on CLAM steel substrates at 300 °C by RF magnetron sputtering, and Si_xC_{1-x} coatings with different Si concentrations were then fabricated on the Al_2O_3 coatings by pulse magnetron sputtering. The coating composition, topography, structure and mechanical properties were investigated by X-ray photoelectron spectroscopy (XPS), atomic force microscopy (AFM), field emission scanning electron microscopy (FE-SEM), X-ray diffractometry (XRD), Raman spectroscopy, nano-indentation techniques and scratch tests. The results show that Si_xC_{1-x} coatings had Si contents in the range 39–62 at.%. Al_2O_3 coatings exhibited an island growth mode, while Si_xC_{1-x} coatings showed a step flow growth mode. Compact and crack-free Si_xC_{1-x}/Al_2O_3 Coatings were prepared. α-Al_2O_3, α-Cr_2O_3 and spinel Fe_2CrO_4 were all detected in the Al_2O_3 coating by Raman spectroscopy. The hardness and elastic modulus of the Al_2O_3 coating were 15.5 ± 1.0 and 194.8 ± 7.2 Gpa, respectively. The hardness and elastic modulus of Si_xC_{1-x} layer were 28.6 ± 0.8 Gpa and 219.2 ± 2.6 Gpa, respectively, for Si content of ≈49 at.%. The adhesion of C-rich and stoichiometric Si_xC_{1-x}/Al_2O_3 coatings were superior to those of Si-rich coatings.

1. Introduction

In the International Thermonuclear Experimental Reactor (ITER) project, the dual-function lithium-lead blanket module (DFLL-TBM) is an attractive design due to its tritium and neutron-breeding capabilities, and also the excellent heat transfer properties of lithium-lead [1]. However, tritium can diffuse through metals and this cannot be completely suppressed by careful choice of a specific metal or alloy. Thus, controlling tritium migration in a facility such as ITER demands particular properties for the choice of blanket structural materials [2,3]. The interaction of radioactive tritium with the fusion reactors structural material is also of great safety concern. An intolerably large pumping power for the metallic coolant in the magnetic field will also be required, because of the MHD (magneto-hydro-dynamic) pressure drop. The pressure reduction will depend on the electric current between the coolant and pipe wall [4,5]. To solve these problems, it is proposed to fabricate an electrically insulating ceramic coating with a large permeation reduction factor (PRF), to segregate the structural walls from the liquid materials.

α-Al_2O_3 has a large PRF and high electrical resistivity, and is a promising candidate for the diffusion barrier coating [6,7]. During most of physical vapor deposition (PVD) or chemical vapor deposition (CVD) processes, α-Al_2O_3 coatings can be prepared with substrate temperatures in excess of 720 °C. Such temperatures are too high for substrates such as steel and glass [3,6,8], and thermal stress in the coatings fabricated at over 720 °C can reduce coating performance [9,10]. However, according to Cloud et al. [11], α-Al_2O_3 films on steel substrate were first to be prepared at 480 °C by AC inverted cylindrical magnetron sputtering. Besides, a template layer with similar lattice constant to α-Al_2O_3 may also be helpful for assisting the low temperature sputtering of α-Al_2O_3. α-Cr_2O_3 ($a_0 = 0.495$ nm) is relatively easy to deposit at low substrate temperatures, and has a lattice mismatch of ≈4.0% with α-Al_2O_3 ($a_0 = 0.476$ nm). Jin et al. [12] and Andersson et al. [13] both reported the use of an α-Cr_2O_3 template layer for the low temperature growth of α-Al_2O_3 films, and the crystallization temperatures decreased to 400 and 280 °C, respectively. Pint and More [14] reported that Al_2O_3 could be transformed to $LiAlO_2$ in Pb–17 at.% Li (a low melting lithium–lead alloy) at 800 °C. The traditional strategy of protecting high temperature alloys by fabricating an Al_2O_3 coating is not always effective. Other metal oxides can also be dissolved in Pb–17 at.% Li. SiC can be stable in eutectic Pb–17 at.% Li up to 800 °C [15–17], which suggests that SiC layers could be used to segregate Pb–17 at.% Li from structural materials. The thermal expansion coefficients of SiC and CLAM (China low activation martensitic) steel are 5.3×10^{-6} and 12.0×10^{-6}/K, respectively. Conversely, the thermal expansion coefficients of SiC and Al_2O_3 (8.8×10^{-6}/K) are much more closely aligned. The adhesion of Al_2O_3 on steel is reasonable, thus if Al_2O_3 coatings can be prepared between SiC and the blanket material, SiC coatings should exhibit better performance.

In the current study, Si_xC_{1-x}/Al_2O_3 coatings with various Si concentrations were prepared by sputtering using a RF magnetron target

* Corresponding author. Tel.: +86 10 62332636; fax: +86 10 62332587.
E-mail address: pingwu@sas.ustb.edu.cn (P. Wu).

0257-8972/$ – see front matter © 2011 Elsevier B.V. All rights reserved.
doi:10.1016/j.surfcoat.2011.03.063

and a pulsed magnetron target. Topographies, structures and mechanical properties of the Al_2O_3 monolayer and Si_xC_{1-x}/Al_2O_3 coatings were investigated.

2. Experimental

A magnetron sputtering system was used to deposit Si_xC_{1-x}/Al_2O_3 coatings on CLAM steel substrates at 300 °C. The sputtering system consisted of two targets. The combined target, formed by silicon stripes (fan-shaped, 99.99 wt.%) radially fixed onto the carbon base target (99.99 wt.%), was powered by a RF power supply with a frequency of 13.56 MHz. The Al (99.99 wt.%) target was powered by a 4 KHz pulsed power supply. The deposition chamber was evacuated to a base vacuum of 1.0×10^{-4} Pa. CLAM steel substrates were polished and then ultrasonically cleaned in acetone, de-ionized water and alcohol, before being fixed on a table. The table was rotated over the two magnetron sputtering sources for the Si_xC_{1-x}/Al_2O_3 coatings. Al_2O_3 layers were prepared from the Al target, while 90 sccm Ar (99.9995%) and 8 sccm O_2 (99.999%) were introduced into the chamber at a pressure of 0.45 Pa. Si_xC_{1-x} layers were prepared from the combined target, while 90 sccm Ar (99.9995%) was introduced into the chamber at a pressure of 0.5 Pa. Samples A, B, C, D and E were prepared as Si_xC_{1-x}/Al_2O_3 coatings from Al and combined targets with P_{Si} (percentage of total target area covered by silicon stripes) of 17, 22, 28, 38 and 44%, respectively.

X-ray photoelectron (XPS) measurements were carried out using a PHI Quantera SXM spectrometer under monochromatic Al Kα radiation (1486.6 eV). Atomic force microscopy (AFM, CPSM500) and field emission scanning electron microscope (FE-SEM, S-4800) were used to characterize the surface and the cross section topographies of the coatings. X-ray diffraction, grazing incident X-ray diffraction (XRD & GIXRD, D/MAX-RB II) and Raman spectroscopy (λ = 514.5 nm, Renishaw Ramanscope, InVia) were used to study the structure of the coatings. Nano-indentation testing was performed at room temperature using a MTS nano indenter dynamic contact module (DCM) system. A Berkovich diamond indenter (three-faced indenter tip) with a half-tip angle of 65.35° was continuously driven into the flat surface of the specimens, with a maximum applied load 19 mN. Scratch tests on the coatings were preformed with a Universal Micro-Tribometer (UMT) using a diamond microblade scratch tool with an edge radius of 200 μm and an acoustic sensor.

3. Results and discussion

3.1. Compositions

XPS was carried out on Al_2O_3 and Al_2O_3/Si_xC_{1-x} coatings, after 5 min of Ar^+ bombardment etching (etching rate ≈ 2.2 nm/min) to remove any surface contamination. XPS results indicated that the atomic ratio of Al to O was approximately 2:3. A near-stoichiometric Al_2O_3 coating was fabricated. Fig. 1 shows the Si 2p and C 1 s spectral regions recorded for samples A, B, C, D and E. Fig. 1a shows that there was only one symmetric peak for the Si 2p region of sample A (P_{Si} = 17%), at 100.4 eV (corresponding to the Si–C bond). With increasing P_{Si}, the Si 2p peak became asymmetric, and Fig. 1b shows a nearly symmetric C 1 s peak for sample E (P_{Si} = 44%). As P_{Si} decreased, the C 1 s peak became asymmetric. The Si 2p peak could be accurately modeled with two Gaussian components: the major component at 100.4 eV was attributed to stoichiometric SiC, and the Si–Si bond was present at 99.3 eV [18]. The C1s peak was also well fitted by two components at 283.3 and 284.4 eV [19], which were attributed to stoichiometric Si – C and C – C bonds, respectively. Fig. 1 shows that SiC and C were both present in sample A. SiC, Si and C were all detected for samples B, C and D. With increasing P_{Si}, the Si – Si bond peak area for the Si 2p peak increased, and the C – C bond peak area for the C1s peak decreased. This suggested that with increasing P_{Si}, Si concentration increased while C concentration decreased. For sample E, the signal of C – Si bond was stronger than that of the C – C bond. The C – C bond was almost negligible, while the Si – Si bond signal was extremely strong.

Fig. 2 shows the Si and C concentrations calculated from Si 2p and C 1 s XPS peaks. The Si concentration was found to increase with P_{Si} at a decreasing rate. The Si_xC_{1-x}coatings' chemical composition can be easily controlled by changing the sputtered area ratio of Si to C. When P_{Si} = 44%, the Si concentration was ≈ 62 %, which was ≈ 1.6 times larger than that of C in Si_xC_{1-x}. This may have been attributed to a higher sputtering yield of Si than C, owing to Si having a lower cohesive energy and a higher energy transfer coefficient [20]. During the deposition of Si_xC_{1-x} coatings, self-bias voltages were also found to increase from 450 to 480 V, as P_{Si} increased from 17 to 44%. Therefore, Ar^+ energy was expected to change simultaneously with self-bias voltage. According to Sigmund's linear collision cascade theory [21], the change of self-bias voltages should be a reason why the Si concentration increased at a decreasing rate.

3.2. Morphologies

Fig. 3 shows the morphologies of Al_2O_3 coating and Si_xC_{1-x}/Al_2O_3 coating with silicon concentration of ≈ 39 at.%. Steps, which were due to their originally rugged condition, were apparent on the substrates. Coating growth was affected by the substrate surface. Fig. 3a shows that there were many coalesced islands on the coating surfaces. Al_2O_3 coating RMS roughness reached 21.3 nm. Fig. 3b shows that step flows with width ≈ 200 nm were present on the surface of Si_xC_{1-x} coating with silicon concentration of ≈ 39 at.%. Besides, the surface morphologies of Si_xC_{1-x}/Al_2O_3 coatings with silicon concentrations ≈ 49, ≈ 55, ≈ 60 and ≈ 62 at.% were also observed by AFM, and they show small difference compared to that with silicon concentration of ≈ 39 at.%. The surfaces of Si_xC_{1-x} with various silicon concentrations were smoother than that of Al_2O_3, with a roughness decreasing to 1.8–4.2 nm. A smooth coating is necessary for optimal mechanical and electrical properties in DFLL-TBM. The results above indicate that a Si_xC_{1-x} coating can help decrease coating roughness. Theoretical and experimental studies have shown that step flow growth is related to growth kinetics, and that step flow is the preferred mode for preparing smooth films [22]. Al_2O_3 and Si_xC_{1-x} were fabricated by different methods and their respective adatoms are quite different. Si_xC_{1-x} coatings are easily prepared with a step flow growth mode using RF magnetron sputtering.

Fig. 4 shows the cross section morphologies of Al_2O_3 coating and Si_xC_{1-x}/Al_2O_3 coatings with silicon concentrations of 39–62 at.%. As shown in Fig. 4a, the thickness of Al_2O_3 was about 1 μm. The Al_2O_3 coating was uniform and compact. In Fig. 4b–f, two layers have been seen: Si_xC_{1-x} layer (with the thickness from 1.1 to 1.8 μm) and Al_2O_3 layer (about 1 μm). Though the composition of Si_xC_{1-x} layers was various, no crack was observed at the Si_xC_{1-x}/Al_2O_3 and the Al_2O_3/substrate interfaces, indicating that the adhesion is expected at the Si_xC_{1-x}/Al_2O_3 and the Al_2O_3/substrate interfaces.

3.3. Microstructures

XRD was used to investigate the Al_2O_3 coating structure. Fig. 5 shows the XRD patterns of the Al_2O_3 coatings on CLAM steel substrate. As shown in Fig. 5a, the Al_2O_3coating's XRD pattern via θ–2θ scanning had small difference compared to that of CLAM steel substrate. A weak peak was observed at 74.4°, which should be induced by α-Al_2O_3. In Fig. 5b, the GIXRD pattern with grazing incidence 5° had an obvious diffraction at 57.5°, attributed to the (116) α-Al_2O_3 plane. XRD has limited sensitivity to microcrystalline or poorly crystalline coating structures. Metallic substrates with fcc, hcp and bcc structures possess only one atom per unique unit cell, and therefore have no Raman-active vibrations [23]. Raman scattering is therefore another approach for studying the structure of ceramic coatings on metallic substrates.

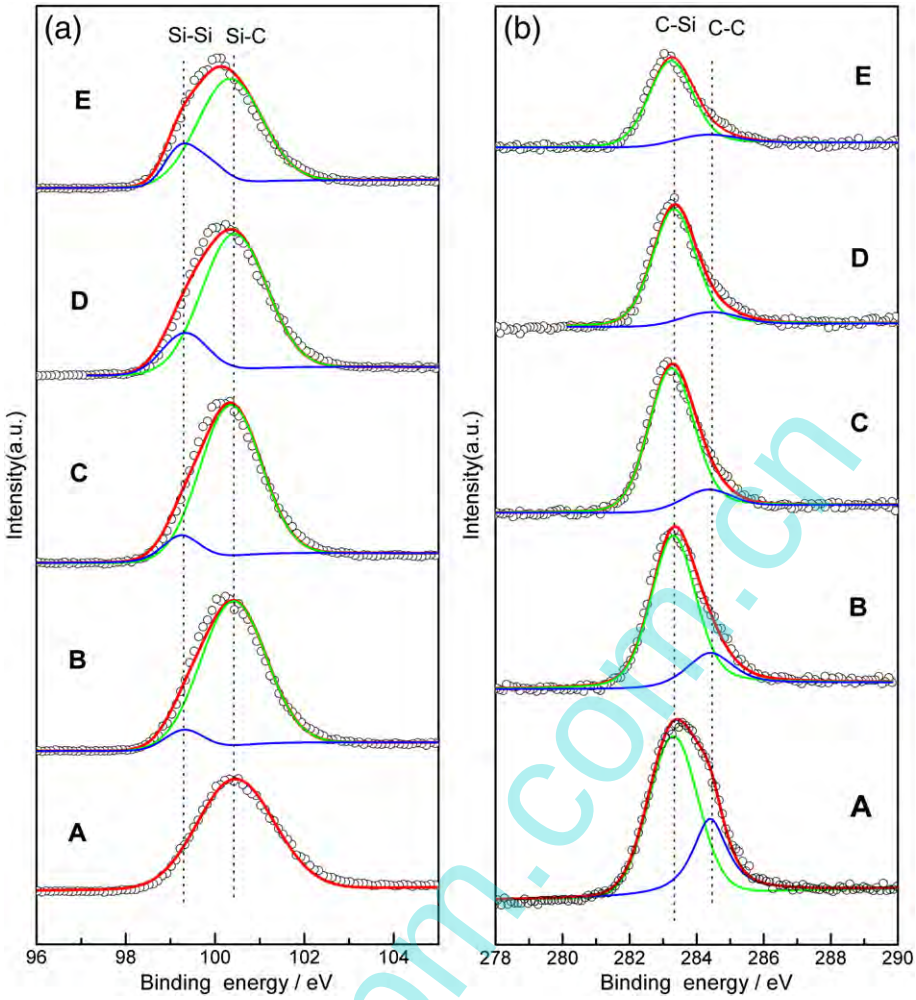

Fig. 1. XPS spectra for samples A, B, C, D, E. (a) Si 2p and (b) C 1 s spectral regions.

Fig. 6 shows the Raman spectrum of the Al_2O_3 coating on CLAM steel, from which broad Raman bands were apparent at 500–800 cm^{-1}. This spectrum was deconvoluted into five bands, all with Gaussian profiles. Raman bands at approximately 577, 645 and 753 cm^{-1} were attributed to α-Al_2O_3 [8,24]. Two further fitted bands at approximately 549 and 685 cm^{-1} were thought to be associated with α-Cr_2O_3 and spinel Fe_2CrO_4 [25].

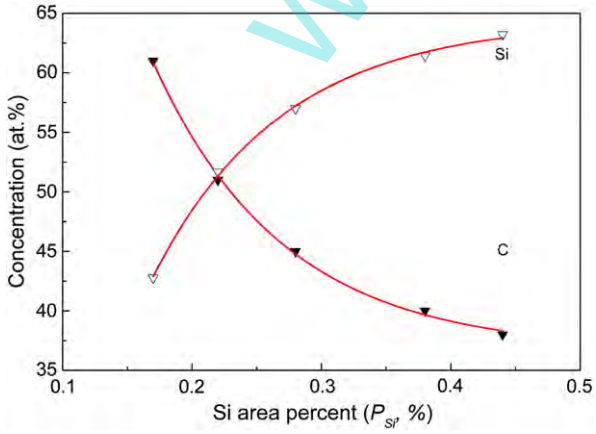

Fig. 2. Si and C concentrations of samples A, B, C, D, E.

In the current study, α-Al_2O_3 could only be fabricated by pulse magnetron sputtering at 300 °C. The Raman spectrum in Fig. 6 shows that α-Cr_2O_3 and spinel Fe_2CrO_4 were also present in the coating layer. Their formation should have been caused by diffusion between the Al_2O_3 coating and CLAM steel substrate (with its high Cr concentration) at the elevated substrate temperature. The formation and presence of α-Cr_2O_3 and spinel Fe_2CrO_4 may have caused a decrease in α-Al_2O_3 crystallization temperature. Moreover, magnetron sputtering is a plasma-activated coating process where the interaction between layer-forming particles and plasma species results in an energetic activation. Plasma density during pulse magnetron sputtering is very high, and coating crystallinity ought to have been enhanced by the plasma activation. Thus, α-Al_2O_3 crystallization temperature could be also decreased by pulse magnetron sputtering.

Fig. 7 shows Raman spectra of Si_xC_{1-x}/Al_2O_3 coatings with various Si concentrations. Spectra of C-rich coatings with Si concentrations of ≈39 and ≈49 at.% exhibited two peaks, which were attributed to the D band (disordered or polycrystalline sp_2 hybridized C) at ≈1336 cm^{-1} and G band (sp_3 hybridized C) at ≈1586 cm^{-1}. There was also a red shifting (Δω) of ≈6 cm^{-1} compared with C–C D and G bands previously reported [26,27]. Si_xC_{1-x}/Al_2O_3 coatings with Si concentrations of ≈60 and ≈62 at.% (in Fig. 7) showed a band at ≈997 cm^{-1}. C–C Raman bands do not usually occur in the 950–1000 cm^{-1} region. Therefore, this band ought to be associated with Si–Si or Si–C bonds. Hobert et al. [28] reported that a broad Raman band at 950–990 cm^{-1} arose from the second-order Raman scattering of Si. The LO peak of 4H–SiC has

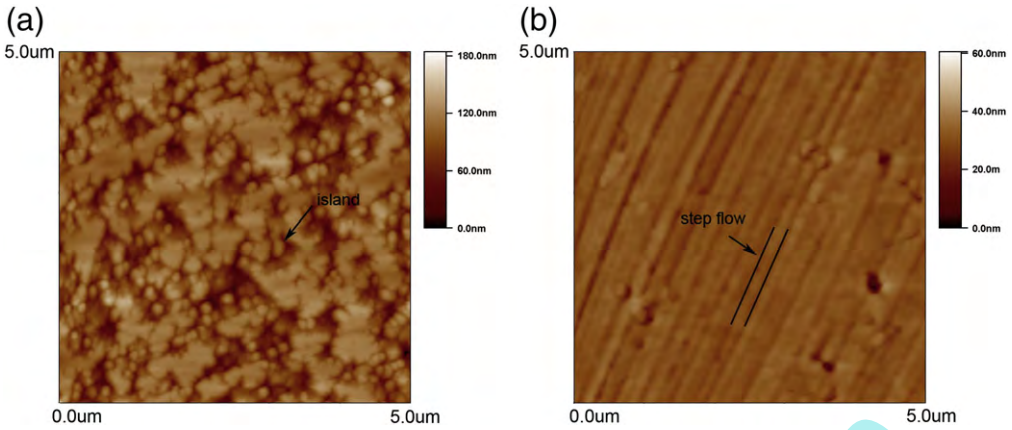

Fig. 3. AFM images of coatings: (a) Al_2O_3, (b) Si_xC_{1-x}/Al_2O_3 coatings with silicon concentration of ≈39 at.%.

also been reported at ≈965 cm^{-1}[29]. Thus it is difficult to ascertain whether the ≈997 cm^{-1} band was due to Si–Si or Si–C bonds. Despite this, there were red shifts observed for Raman bands of Si_xC_{1-x}/Al_2O_3 coatings with Si concentrations of ≈60 and ≈62 at.%. Bands can shift due to changes in measurement, temperature, applied external pressure, sample stress, degree of stacking disorder, coupling with electron plasmon mode, etc. Coating materials' compressive stress, caused by the lattice and mismatch between thermal expansion coefficients, is also a major factor causing red shifting in Raman spectra [30]. The thermal expansion coefficient of the CLAM steel substrate was larger than that of the ceramic coating, and red shifts were probably predominantly caused by compressive stress in Si_xC_{1-x}/Al_2O_3 coatings.

Fig. 8 shows the XRD patterns of Si_xC_{1-x}/Al_2O_3 coatings with various Si concentrations. In Fig. 8a, as the silicon concentration of the Si_xC_{1-x} layers increases from ~55 at.% to ~60 at.%, a peak at 43.5° is sensibly broadened toward lower 2θ, according to a metastable tetragonal Si super lattice peak of (320) [31]. Based on the XRD results, the Raman band, observed at ≈997 cm^{-1} (shown in Fig. 8), should be induced by Si–Si band in the Si rich coatings.

3.4. Mechanical properties

Nano-indentation tests were performed to measure the hardness and elastic modulus of the coatings. The indentation depth was kept at a constant of 230 nm. For the purpose to avoid the influence of the substrate, the hardness and the elastic modulus were obtained at the depth of 1/10 thickness of Al_2O_3 or Si_xC_{1-x} layers [32]. The hardness and the elastic modulus of Al_2O_3 coating were found to be 15.5 ± 1.0 and 194.8 ± 7.2 Gpa, respectively. Fietzke et al. [33] reported that the

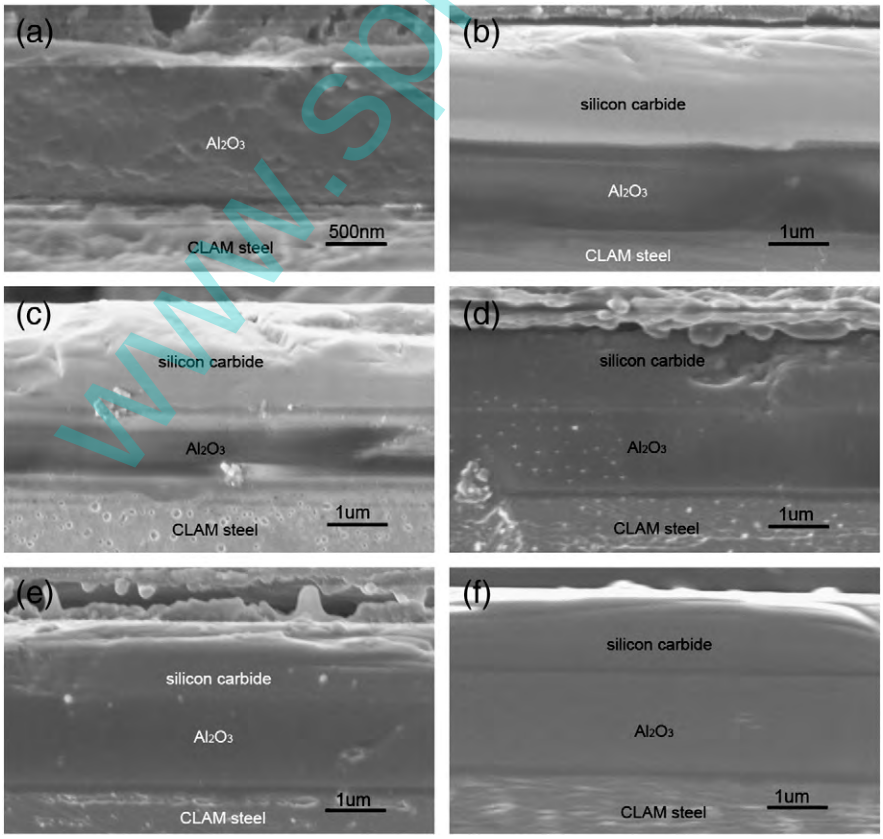

Fig. 4. FE-SEM cross section observation: (a) Al_2O_3 coating; and (b)-(f) Si_xC_{1-x}/Al_2O_3 coatings with silicon concentrations of (b) ≈39, (c) ≈49, (d) ≈55, (e) ≈60 and (f) ≈62 at.%.

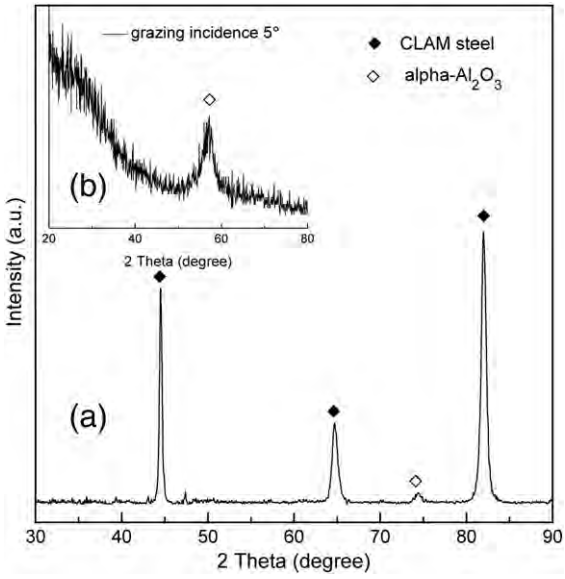

Fig. 5. XRD patterns of CLAM steel substrate and Al_2O_3 monolayer: (a) via θ–2θ scanning; (b) with grazing incidence 5°.

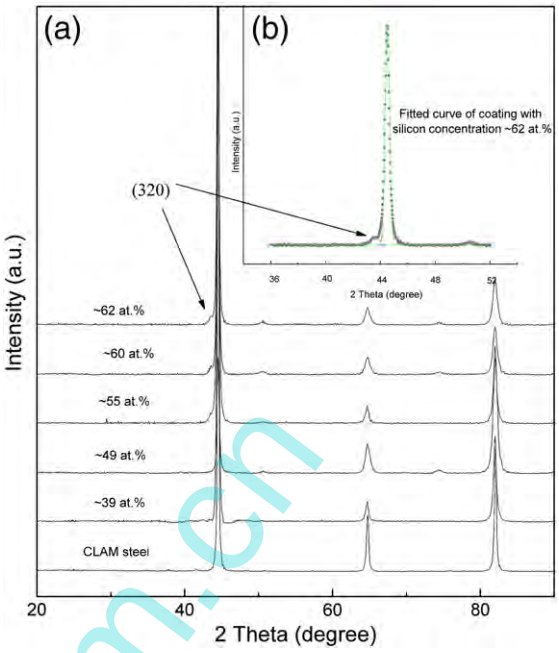

Fig. 8. XRD patterns of (a): CLAM steel substrate and Si_xC_{1-x}/Al_2O_3 coatings with various silicon concentrations; (b): Fitted curve of Si_xC_{1-x}/Al_2O_3 coatings with silicon concentration of ~62 at.%

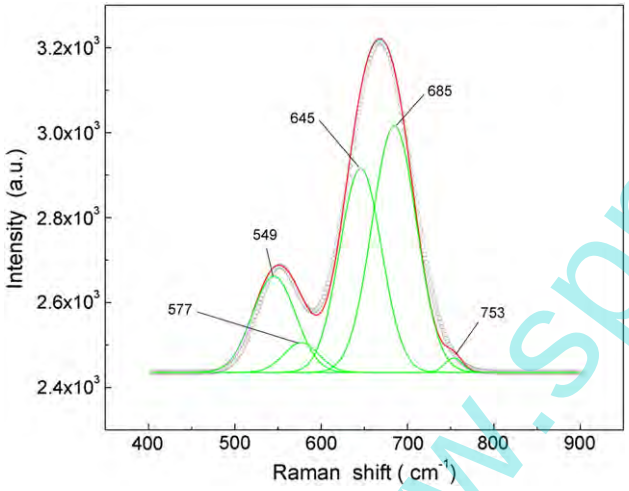

Fig. 6. Raman spectrum of Al_2O_3 monolayer on CLAM steel.

hardness of pure α-Al_2O_3 and amorphous Al_2O_3 coatings, fabricated by pulse magnetron sputtering on tool steel substrates, were 22 and 7–12 GPa, respectively. Thus, the hardness of Al_2O_3 coatings fabricated in this study was between those of pure alpha and amorphous Al_2O_3 coatings. Degree of crystallization is an important factor affecting coating hardness, and poor crystallinity may have resulted in a lower coating hardness than expected.

Fig. 9 shows the hardness and elastic modulus of Si_xC_{1-x} layers as a function of Si concentration. The hardness and elastic modulus were obtained at the depth of 1/10 thickness of Si_xC_{1-x} layers. Si_xC_{1-x} layer hardness was more than 20 GPa, which was considerably higher than that for the Al_2O_3 coating. Si_xC_{1-x} layer hardness reached a maximum of 28.6 ± 0.8 Gpa at Si concentration of $\approx$49 at.%. Fig. 9 also shows that the elastic modulus reached a maximum when the Si concentration was $\approx$55 at.%. Hence, a stoichiometric Si_xC_{1-x} layer was necessary for high hardness and elastic modulus.

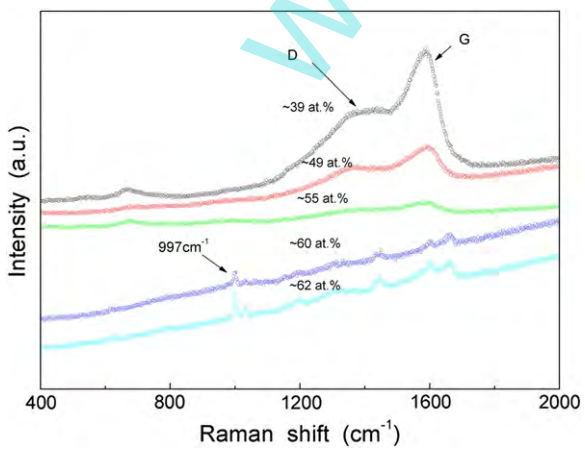

Fig. 7. Raman spectra for Si_xC_{1-x}/Al_2O_3 bilayers with various silicon concentrations.

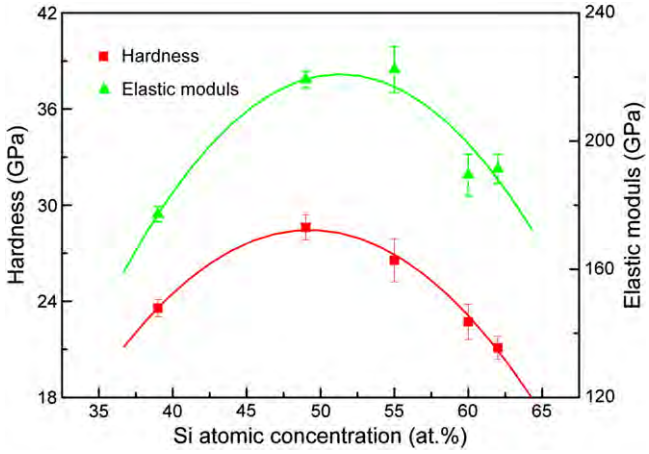

Fig. 9. Hardness and elastic modulus of Si_xC_{1-x} layers as a function of Si concentration.

Table 1
The critical loads of Al_2O_3 coating and samples A, B, C, D, E (with silicon concentrations of sample A ≈ 39, B ≈ 49, C ≈ 55, D ≈ 60 and E ≈ 62 at.%.).

Samples	Al_2O_3	Sample A	Sample B	Sample C	Sample D	Sample E
Critical load	7.9 ± 0.2	6.2 ± 0.2	6.5 ± 0.3	5.2 ± 0.1	4.8 ± 0.1	3.4 ± 0.3

The adhesive properties of the Al_2O_3 and the Si_xC_{1-x}/Al_2O_3 coatings on CLAM steel substrates were studied by UMT. The normal load on the microblade was increased from 3 N to 14 N over 70 S, while the blade moved at a constant speed of 0.086 mm/s and total sliding distance of 6 mm. The adhesion strength of the coating was determined from the critical load at which the acoustic signal exhibited a large increase in fluctuations as a result of coating delamination [34].

Table 1 shows the critical loads of Al_2O_3 and Si_xC_{1-x}/Al_2O_3 coatings on CLAM steel substrates. Though the critical loads of Si_xC_{1-x}/Al_2O_3 coatings on CLAM steel substrates were all less than that of Al_2O_3 coatings, Si_xC_{1-x}/Al_2O_3 critical loads reached 6.2 N and 6.5 N at Si concentration of ≈39 at.% and ≈49 at.%. While the Si concentration was equal or greater than 55 at.%, the critical load decreased obviously with Si concentration. This indicated that the adhesion strength between Al_2O_3 and Si-rich Si_xC_{1-x} layers was relative lower. An excess of Si in Si_xC_{1-x}/Al_2O_3 coating could reduce the adhesion.

4. Conclusions

Si_xC_{1-x}/Al_2O_3 coatings with Si concentrations of 39–62 at.% were prepared on CLAM steel by magnetron sputtering. Al_2O_3 was formed by an island growth mode, while the Si_xC_{1-x} layer had a step flow growth mode. Compact Si_xC_{1-x}/Al_2O_3 coatings had been prepared, and almost no crack was observed at the Si_xC_{1-x}/Al_2O_3 and Al_2O_3/CLAM steel interfaces. XRD and Raman spectra showed that the Al_2O_3 layer possessed a crystalline α-Al_2O_3 phase. Besides, α-Cr_2O_3 and spinel Fe_2CrO_4 were also detected. Al_2O_3 coating crystallinity may have been related to Cr_2O_3 and Fe_2CrO_4 formation. Raman spectra of coatings with Si concentrations of ≈60 and ≈62 at.% had a band at ≈997 cm^{-1}, which should be caused by redundant Si. The hardness and elastic modulus of the Al_2O_3 coating were 15.5 ± 1.0 and 194.8 ± 7.2 Gpa, respectively. Si_xC_{1-x} layers with maximum hardness and elastic modulus values had Si concentrations of ≈49 and ≈55 at.%, respectively. An excess of Si in Si_xC_{1-x}/Al_2O_3 coating reduced the adhesion of the coatings.

Acknowledgment

We would like to thank the National Natural Science Foundation of China for financial support (No. 50776010).

References

[1] C.P.C. Wong, V. Chernov, A. Kimura, Y. Katoh, N. Morley, T. Muroga, K.W. Song, Y.C. Wu, M. Zmitko, J. Nucl. Mater. 367–370 (2007) 1287.
[2] H. Nakamura, M. Nishi, J. Nucl. Mater. 329–333 (2004) 183.
[3] R. Brill, F. Koch, J. Mazurelle, D. Levchuk, M. Balden, Y. Yamada-Takamura, H. Maier, H. Bolt, Surf. Coat. Technol. 174–175 (2003) 606.
[4] S. Malang, H.U. Borgstedt, E.H. Farnum, K. Natesan, I.V. Vitkovski, Fusion Eng. Des. 27 (1995) 570.
[5] A. Sawada, T. Terai, A. Suzuki, M. Yamawaki, J. Phys. Chem. Solid. 66 (2005) 681.
[6] D. Levchuk, F. Koch, H. Maier, H. Bolt, J. Nucl. Mater. 328 (2004) 103.
[7] P. Frach, H. Bartzsch, D. Glöß, M. Fahland, F. Händel, Surf. Coat. Technol. 202 (2008) 5680.
[8] V. Edlmayr, M. Moser, C. Walter, C. Mitterer, Surf. Coat. Technol. 204 (2010) 1576.
[9] A.K. Costa, S.S. Camargo, Surf. Coat. Technol. 163–164 (2003) 176.
[10] M.I. Jones, I.R. McColl, D.M. Grant, K.G. Parker, T.L. Parker, J. Biomed. Mater. Res. 52 (2000) 413.
[11] A.N. Cloud, S. Canovic, H.H. Abu-Safe, M.H. Gordon, M. Halvarsson, Surf. Coat. Technol. 203 (2008) 808.
[12] P. Jin, G. Xu, M. Tazawa, K. Yoshimura, D. Music, J. Alami, U. Helmersson, J. Vac, Sci. Technol. A. 20 (2002) 2134.
[13] J.M. Andersson, Z. Czigany, P. Jin, U. Helmersson, J. Vac, Sci. Technol. A. 22 (2004) 117.
[14] B.A. Pint, K.L. More, J. Nucl. Mater. 376 (2008) 108.
[15] S. Zhao, X. Zhou, H. Yu, H. Wang, Y. Wu, Q. Huang, Z. Zhu, Z. Huang, Fusion Eng. Des. 85 (2010) 1624.
[16] H. Kleykamp, J. Nucl. Mater. 321 (2003) 170.
[17] P. Wang, J. Liu, Y. Wang, B. Shi, Surf. Coat. Technol. 128–129 (2000) 99.
[18] K. Xue, L.-S. Niu, H.-J. Shi, J. Liu, Thin Solid Films 516 (2008) 3855.
[19] D. Song, E.-C. Cho, G. Conibeer, Y.-H. Cho, Y. Huang, S. Huang, C. Flynn, M.A. Green, J. Vac, Sci. Technol. B. 25 (2007) 1327.
[20] H. Lutz, M. Bruns, F. Link, H. Baumann, Surf. Coat. Technol. 116–119 (1999) 419.
[21] P. Sigmund, Phys. Rev. 184 (1969) 383.
[22] M. Yoon, H.N. Lee, W. Hong, H.M. Christen, Z. Zhang, Z. Suo, Phys. Rev. Lett. 99 (2007) 055503.
[23] J.A. Creighton, R. Withnall, Chem. Phys. Lett. 326 (2000) 311.
[24] P.G. Li, M. Lei, W.H. Tang, Mater. Lett. 64 (2010) 161.
[25] C.F. Windisch Jr., C.H. Henager Jr., M.H. Engelhard, W.D. Bennett, J. Nucl. Mater. 383 (2009) 237.
[26] M. Kuenle, S. Janz, O. Eibl, C. Berthold, V. Presser, K.-G. Nickel, Mater. Sci. Eng. B. 159–160 (2009) 355.
[27] J.E. Proctor, E. Gregoryanz, K.S. Novoselov, M. Lotya, J.N. Coleman, M.P. Halsall, Phys. Rev. B 80 (2009) 073408.
[28] H. Hobert, H.H. Dunken, J. Meinschien, H. Stafast, Vib. Spectrosc. 19 (1999) 205.
[29] S. Nakashima, T. Kitamura, T. Kato, K. Kojima, R. Kosugi, H. Okumura, H. Tsuchida, M. Ito, Appl. Phys. Lett. 93 (2008) 121913.
[30] M. Bosi, B.E. Watts, G. Attolini, C. Ferrari, C. Frigeri, G. Salviati, A. Poggi, F. Mancarella, A. Roncaglia, O. Martinez, V. Hortelano, Cryst. Growth Des. 9 (2009) 4852.
[31] Y.-X. Zhao, F. Buehler, J.R. Sites, I.L. Spain, Solid State Commun. 59 (1986) 679.
[32] N.G. Chechenin, J. Bøtiger, J.P. Krog, Thin Solid Films 261 (1995) 219.
[33] F. Fietzke, K. Goedicke, W. Hempel, Surf. Coat. Technol. 86–87 (1996) 657.
[34] K. Jagannadham, T.R. Watkins, M.J. Lance, L. Riester, R.L. Lemaster, Surf. Coat. Technol. 203 (2009) 3151.